A theoretical scenario for the mechanical failure of boron carbide nanotubes

Azam Salmankhani, Zohre Karami, Amin Hamed Mashhadzadeh, Maryam Zarghami Dehaghani, Mohammad Reza Saeb, Vanessa Fierro, Alain Celzard, Mohammad Reza Saeb

A theoretical scenario for the mechanical failure of boron carbide nanotubes

Azam Salmankhani [1], Zohre Karami [2], Amin Hamed Mashhadzadeh [2]*, Maryam Zarghami Dehaghani [2], Mohammad Reza Saeb [2], Vanessa Fierro [3], Alain Celzard [3,†]

[1] Faculty of Mechanical Engineering, K. N. Toosi University of Technology, Tehran, Iran; azamsalmankhani@gmail.com; P.O.Code: 1969764499

[2] Center of Excellence in Electrochemistry, School of Chemistry, College of Science, University of Tehran, P.O. Box: 14155-6455, Tehran, Iran; zohrekarami.2013@yahoo.com & amin.hamed.m@gmail.com & maryam_zz67@yahoo.com & mrsaeb2008@gmail.com

[3] Université de Lorraine, CNRS, IJL, F-88000 Epinal, France; vanessa.fierro@univ-lorraine.fr & alain.celzard@univ-lorraine.fr

* Correspondence: amin.hamed.m@gmail.com , amin.hamedmashhadzadeh@yahoo.com; Tel.: (+98-9113765114)

† Correspondence: alain.celzard@univ-lorraine.fr; Tel.: (+33-372-74-9614)

Abstract

Although the volume of research on carbon nanotubes (CNTs) has increased over a short period, less attention has been paid to other types of carbon-based nano-objects such as boron carbide (BC_3) nanotubes (BC_3NTs). In the present article, we modeled BC_3NTs using molecular dynamics (MD) simulation to investigate the effects of chirality, wall number, diameter and temperature on the mechanical failure of BC_3NTs, BC_3 nanobuds and BC_3NTs with different kinds of defects. In addition, we modeled the corresponding CNTs to validate the results and understand how the replacement of a quarter of the carbon atoms in the CNT by boron atoms affects the properties of the newly formed nanotube. The results showed that the variation of mechanical properties as a function of diameter and temperature was rather limited, regardless of chirality. The Young's modulus, failure stress and failure strain of the zigzag single-walled BC_3NTs ($SWBC_3$NTs) were lower than the armchair ones, and were lower than those of the corresponding CNTs too. Furthermore, adding a second and third wall to the $SWBC_3$NTs significantly improved their mechanical properties. Finally, we modeled BC_3 nanobuds with 1 to 4 C_{60} attached to the surface of $SWBC_3$NTs and observed that the properties decreased as the number of fullerenes increased. Moreover, considering defective $SWBC_3$NTs revealed that two-atom vacancies and Stone-Wales defects resulted in the highest and lowest reduction of mechanical properties, respectively.

Keywords: BC_3 nanotubes; Molecular Dynamics; Mechanical Properties; Nanobud; Defect

1. Introduction

Carbon nanotubes (CNTs) are best known for their excellent mechanical strength, high thermal and electrical conductivity and good sensing capability, making them excellent candidates for the development of technical materials and systems (see Figure 1S in the Supplementary Information, SI) [1, 2]. Chemical doping with heteroelements is a promising technique for improving their mechanical, electronic, optical and chemical properties [3-8]. A particular type of boron-doped CNTs can be obtained when a quarter of the carbon in the graphene is replaced by boron atoms, resulting in a new structure called BC_3 graphene. Like CNTs, BC_3 nanotubes (BC_3NTs) are formed when a BC_3 sheet is wound along its chiral vector [9-11]. For BC_3 compounds, only the B-C and C-C bonds are considered stable, while the B-B bonds are neglected because they are less stable. BC_3 nanosheets have good temperature resistance and are of high crystalline quality [12].

The mechanical properties and failure mechanism of the nanostructures are of great importance, particularly at high temperatures [13, 14]. Although BC_3NTs have been extensively studied from an electronic or chemical perspective, less attention has been paid to understanding the mechanical failure of BC_3NTs. In a recent work, we have modeled and simulated the mechanical properties of either defect-free or defective C_3N nanotubes (C_3NNTs) and their nanobuds, and analyzed and compared the results with the corresponding modeled CNTs as a reference/control geometry for validation [15].

In this framework, we have developed BC_3 nanotubes by replacing a quarter of the CNTs atoms with boron atoms in order to explore the effect of chirality, tube diameter, number of walls and temperature on the elastic modulus, failure stress and failure strain of flawless and defective BC_3NTs, as well as BC_3 nanobuds. Since no research has reported on the mechanical properties of BC_3NTs, the results of our previous work on corresponding CNTs with the same chirality and under the same loading conditions have been considered as a

reference to theoretically validate our new results obtained by Molecular Dynamics (MD) simulation [15].

2. Computational design

The molecular dynamics modeling in the present study was performed using the large-scale atomic/molecular massively parallel simulator (LAMMPS) package to predict the mechanical properties of BC_3NTs in either armchair or zigzag chirality. To model C-C bonds, we selected the modified Tersoff potential presented by Lindsay and Broido [16]. Moreover, to define the interaction of carbon and boron atoms, we used the Tersoff potential parameters developed by Kinaci et al. [17]. Armchair and zigzag BC_3NTs with an approximate length of 5 nm were modeled and the results obtained were compared with those of the corresponding carbon nanotubes (CNTs) as reference materials from our previous article [15]. To calculate the mechanical properties, the stress-free structures at the simulated temperature were first performed with the isothermal-isobaric (NPT) ensemble at 300 K (pressure of 1 bar) with the time span of 100 ps. Next, the simulation box was stretched along the loading axial direction (z-direction) with the strain rate of 10^9 s^{-1}. To measure the effects of temperature, single-walled nanotubes in either zigzag or armchair chirality were modeled and tested at temperatures varying from 300K to 900K. Besides, the effects of wall addition, fullerene attachment, and different types of defects on the elastic modulus, failure stress and failure strain of BC_3 nanotubes were determined under the same loading conditions. We have provided a brief flowchart of the total modeling process used in the present study in Figure 1. This flowchart follows the same procedure as that used in our previous article [15].

3. Results and discussion

3.1. Mechanical properties of single-walled BC_3NTs

To study the mechanical properties, we first modeled zigzag and armchair single-walled BC_3 nanotubes ($SWBC_3NTs$) and their corresponding CNTs using molecular dynamics (MD) simulation. A schematic of the modeled $SWBC_3NTs$ and their stoichiometry are shown in Figure S2 and Table 1, both derived from the reference materials [15]. The values of radius corresponding to each chirality are tabulated in Table S1. In Figure S2 and Table 1, $DWBC_3NTs$ and $TWBC_3NTs$ refer to double-walled and triple-walled nanotubes, respectively. Next, all samples were subjected to uniaxial tensile loading with a strain rate of 0.001 ps^{-1} when the temperature was set at 300K, and the stress-strain ($\sigma - \varepsilon$) curves were extracted to calculate Young's modulus, failure stress, and failure strain. A schematic view of a (8,0) zigzag BC_3NT under uniaxial tensile loading is shown in Figure S3.

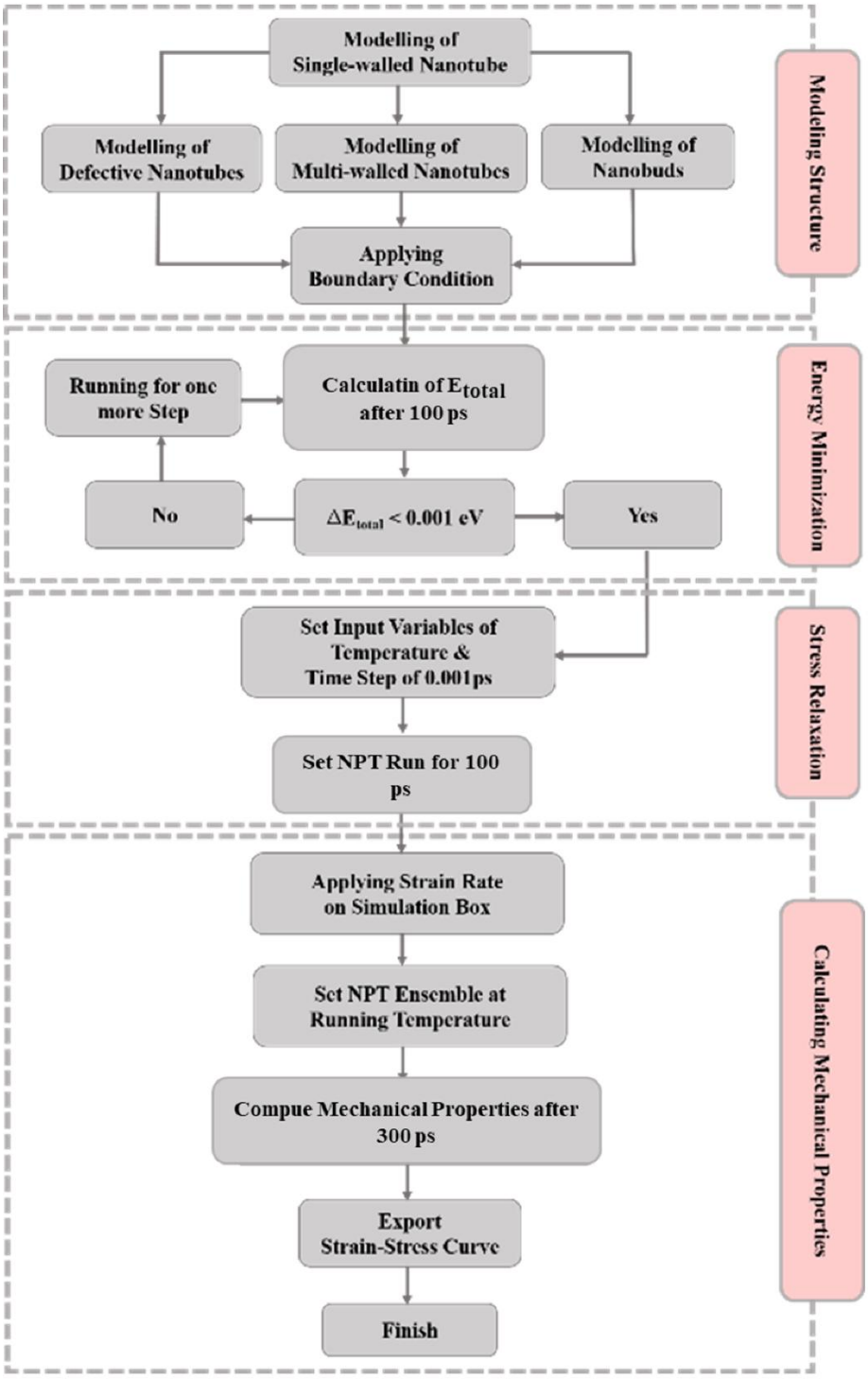

Figure 1. Flowchart of the overall simulation steps including modeling, energy minimization and calculation of properties.

105

Table 1. Stoichiometry and chirality of $SWBC_3NTs$, $DWBC_3NTs$, $TWBC_3NTs$.

Chirality	Number of Atoms	Chirality	Number of atoms
(4,4)	328	(4,4),(7,7)	902
(6,6)	492	(4,4),(8,8)	984
(8,8)	656	(4,4),(9,9)	1066
(10,10)	820	(4,4),(10,10)	1148
(12,12)	984	(4,4),(11,11)	1230
(8,0)	384	(4,4),(12,12)	1312
(10,0)	480	(8,0),(14,0)	1056
(12,0)	576	(8,0),(16,0)	1152
(14,0)	672	(8,0),(18,0)	1248
(16,0)	768	(8,0),(20,0)	1344
(18,0)	864	(4,4),(8,8),(12,12)	1968
(20,0)	960	(8,0),(14,0),(20,0)	2016

106

107 To obtain the Young's modulus, a second-order polynomial was fitted to the linear part
108 of the stress-strain curves using the following equation [18].

$$\sigma = \frac{\partial U}{\partial \varepsilon} = D\varepsilon^2 + E\varepsilon + C \quad (1)$$

109 where *E*, *D*, and *C* are the Young's modulus, third-order elastic modulus and residual stress
110 of the nanotubes, respectively. A stress-strain curve plotted for a (6,6) armchair BC_3NT is
111 presented in Figure 2a, and Figure 2b shows a zoom of the linear part of the plot used for the
112 second-order polynomial fit. As seen in Figure 2a, the highest stress obtained is observed at a
113 strain rate of about 40%. Then, the stress drops to a considerably lower amplitude. Therefore,
114 the coordinates of this point correspond to the values of failure stress and failure strain.

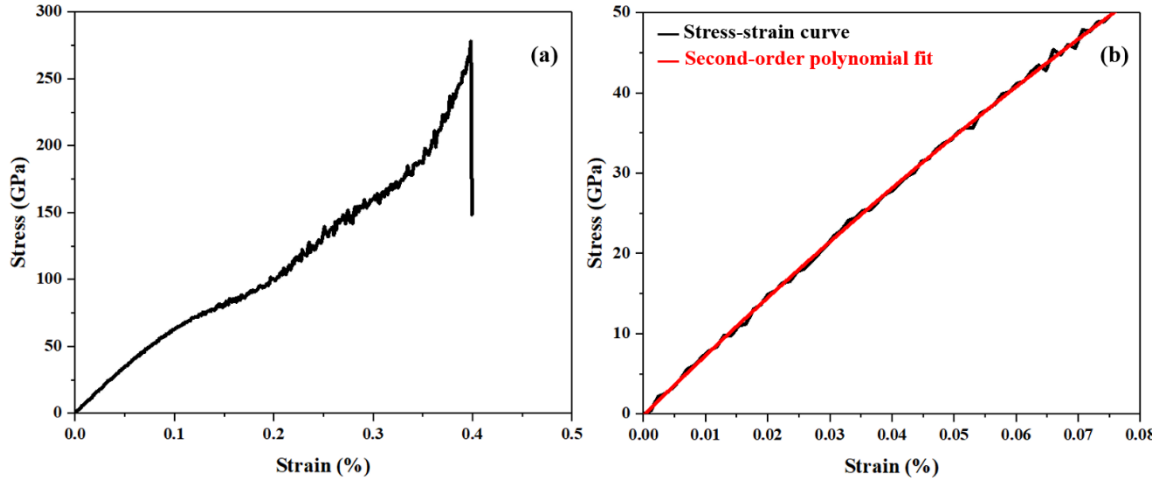

Figure 2. (a) Stress-strain curve for a (6,6) armchair BC_3NT, and **(b)** zoom on the second-order polynomial fit.

The same steps were repeated for all $SWBC_3NTs$ and the plots of the mechanical properties are shown in Figure 3. According to Figure 3a, the Young's modulus of $SWBC_3NTs$ is significantly lower than those of the reference SWCNTs [15], either in zigzag or armchair structure. This could be associated with the stronger C-C bonds of CNTs compared to B-C bonds of BC_3NTs due to the shorter C-C bond (144.1 pm) compared to B-C bond (153.5 pm). Furthermore, the Young's modulus of armchair $SWBC_3NTs$ was slightly higher than zigzag structures of close radius. By increasing the size of the nanotubes, the elastic modulus of armchair $SWBC_3NTs$ increased slightly from 724.8 GPa in structure (4,4) to the maximum value of 780.5 GPa in structure (10,10) and then decreased to 776.7 GPa in structure (12,12). Similarly, an upward behavior was observed in zigzag $SWBC_3NTs$, i.e., the Young's modulus increased from the lowest value of 718.4 GPa in structure (8,0) to the highest value of 751.7GPa in structure (16,0), and then decreased slightly to 741.5 GPa in structure (20,0). By increasing the radius, the elastic modulus of the armchair and zigzag $SWBC_3NTs$ increased by approximately 7% and 4%, respectively. The same behavior was observed for the Young's modulus of armchair SWCNTs while zigzag SWCNTs remained almost unchanged by increasing the radius of nanotubes [15]. The results previously obtained [15] with armchair and zigzag SWCNTs as reference materials were in the range of 1 TPa,

which is close to other data [19-21], thereby demonstrating the accuracy of the used model and the obtained results for $SWBC_3NTs$. In their experimental study, Yu et al. reported the average modulus obtained for 8 SWCNT ropes using atomic force microscopy, equal to 1002 GPa [22]. Furthermore, Treacy et al. calculated an elastic modulus in the range of 2TPa for individual SWCNTs of different lengths and radii [23]. Moreover, the failure stress plots in Figure 3b reveal that armchair $SWBC_3NTs$ have higher stress at break than zigzag $SWBC_3NTs$ (almost three times as high), and the same behavior was observed in armchair SWCNTs compared to zigzag ones as derived from reference samples [15]. The results obtained for armchair and zigzag $SWBC_3NTs$ and their corresponding SWCNTs are gathered in Tables S2 and S3, respectively.

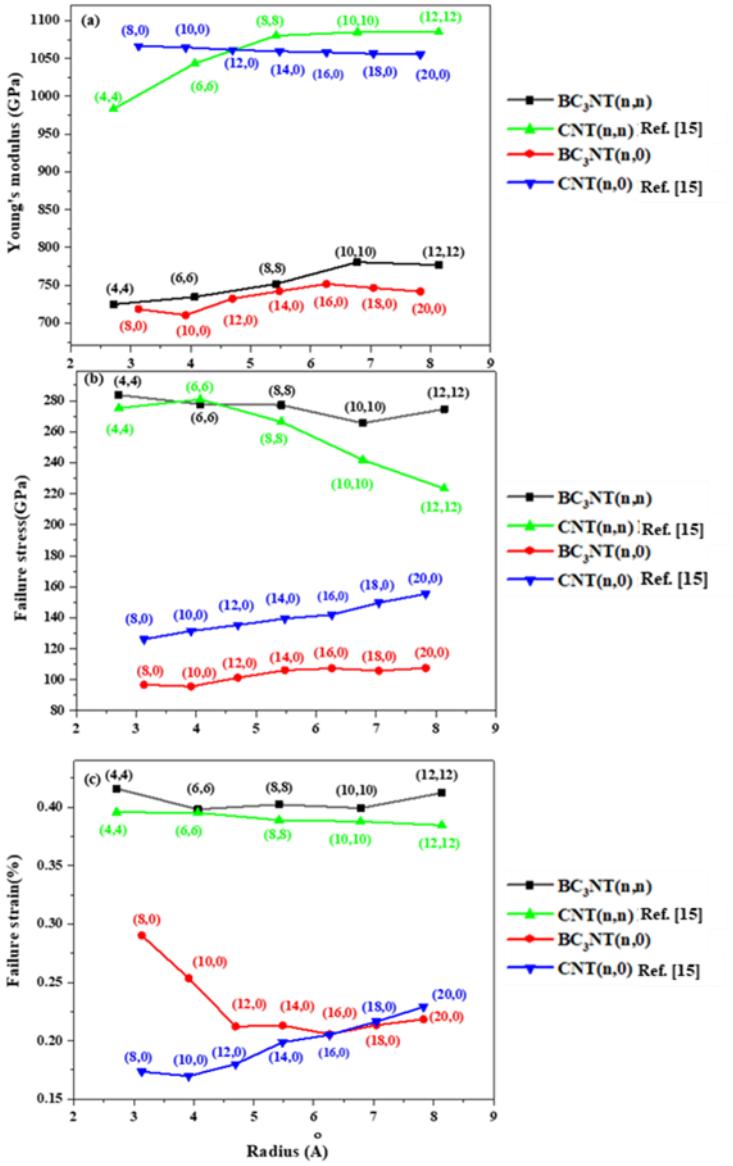

Figure 3. (a) Young's modulus, **(b)** failure stress and **(c)** failure strain of armchair and zigzag structures of SWBC$_3$NTs under uniaxial tensile tests at 300K and their corresponding reference SWCNTs materials (from [15]).

In addition, by increasing the radius of the nanotubes, the failure stress of the armchair SWBC$_3$NTs slowly decreased, while on the other hand, the failure stress of zigzag SWBC$_3$NTs increased (in the limits of certain fluctuations). The highest failure stress of the armchair and zigzag SWBC$_3$NTs obtained was observed in structures (4,4) and (20,0) with values of 283.71 GPa and 107.6 GPa, respectively. Figure 3c shows the failure strain of the SWBC$_3$NTs and their corresponding reference SWCNTs (from [15]). According To this

figure, and as already noted for elastic modulus and failure stress, the failure strain of zigzag and armchair $SWBC_3NTs$ was higher than or very close to that of SWCNTs with close radius, and the failure strain of the armchair $SWBC_3NTs$ was higher than that of the zigzags. While the failure strain of the armchair $SWBC_3NTs$ and SWCNTs was almost unchanged, this property decreased significantly from the highest value of 0.295% in zigzag structure (8,0) to the lowest value of 0.205% in structure (16,0), followed by a small increase to 0.218% in structure (20,0). Overall, armchair $SWBC_3NTs$ exhibited higher mechanical properties than zigzag $SWBC_3NTs$.

To understand the effects of temperature on the mentioned properties, we selected a zigzag and an armchair $SWBC_3NT$ with the closest radius, of structures (18,0) and (10,10), respectively, and examined their properties while the temperature was varied from 300K to 900K as shown in Figure 4. We also used the results of our previous article for comparison with reference CNTs subjected to the same range of temperature [15]. This figure shows that temperature had a negative effect on the mechanical properties of both $SWBC_3NTs$ and SWCNTs. The Young's modulus of the armchair $SWBC_3NTs$ indeed constantly decreased from 780.5 GPa at 300K to 711.2 GPa at 900K (i.e., by 8%) while the modulus of zigzag $SWBC_3NTs$ was reduced from 746.4 GPa at 300K to 668.4 GPa at 900K (i.e., by 10%). Besides, Figures 4b and 4c reveal that, although the failure stress and failure strain of the armchair $SWBC_3NTs$ and SWCNTs were higher than for the corresponding zigzag structures at lower temperatures, these properties decreased sharply in armchair structures, reaching a lower value at higher temperatures compared to zigzag $SWBC_3NTs$ or SWCNTs. The minimum failure stress and failure strain were found in armchair $SWBC_3NTs$ at 900K with values of 76.85 GPa and 0.14%, respectively. The same kind of results were observed by Zahedi et al. for BC_3 single-layers [24]. They found that the Young's modulus of BC_3

single-layers decreased by about 10% and 3% in armchair and zigzag directions at 900K compared to 200K, respectively.

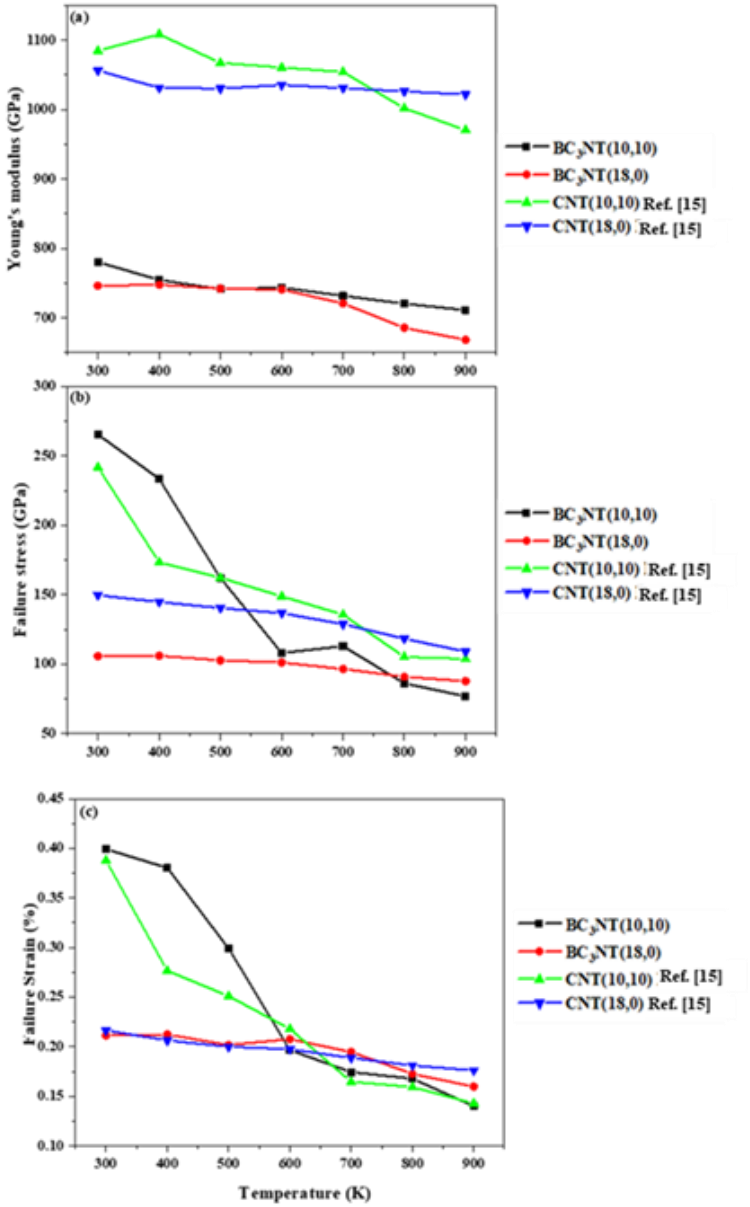

Figure 4. (a) Young's modulus, **(b)** failure stress and **(c)** failure strain of (10,10) and (18,0) $SWBC_3NTs$ and SWCNTs reference materials (from [15]) under uniaxial tensile tests as a function of temperature.

3.2. Mechanical properties of double-walled BC_3NTs

In order to determine the effects of wall addition on the mechanical properties of $SWBC_3NTs$, six armchair and four zigzag double-walled ($DWBC_3NTs$) were modeled and tested, and the results were compared with those of the corresponding reference CNTs from

[15]. A schematic view of the designed $DWBC_3NTs$ is displayed in Figure S4, and the results of Young's modulus, failure stress and failure strain are presented in Figure 5. All tests were implemented at a constant temperature of 300K while the samples were subjected to uniaxial tensile loading. It should be mentioned that there are some limitations for modeling multi-walled nanotubes regarding interlayer distance. If the distance between layers exceeds a critical value, see Figure S5 for upper and lower limits of interlayer distance, no van der Waals interaction can take place between the layers and therefore no stable structure is formed. Otherwise, when the interlayer distance is below a certain value, the structure is unstable and collapses. Consequently, the distances shown in Figure S4 were selected to model stable armchair and zigzag structures with similar dimensions.

Figure 5a shows that by increasing the radius of the nanotubes, which is the consequence of the increase of the interlayer distance, the Young's modulus progressively decreased in both $DWBC_3NTs$ and reference DWCNTs samples from [15]. The elastic modulus of two of the zigzag $DWBC_3NTs$ including structures (8,0),(14,0) and (8,0),(16,0) was higher than those for armchair $DWBC_3NTs$ of a similar radius, including structures (4,4),(7,7) and (4,4),(8,8), and two others had a lower modulus than the corresponding armchairs $DWBC_3NTs$. The maximum Young's modulus of the armchair and zigzag $DWBC_3NTs$ were 1122.9 GPa and 1094.4 GPa, obtained for structures (8,0),(16,0) and (4,4),(8,8), respectively, and this property was about 8% and 5% lower in the thicker zigzag and armchair $DWBC_3NTs$ compared to the thinner ones. Comparison of the Young's modulus of $DWBC_3NTs$ and DWCNTs reveals the higher modulus of DWCNTs. The highest Young's modulus of DWCNTs was 1553.3 GPa, calculated for the structure (8,0),(16,0). This value is within the range of previous reports for DWCNTs, thus supporting the accuracy of the results of this study [25, 26].

Unlike Young's modulus, the failure stress of armchair $DWBC_3NT$ and DWCNT did not change significantly, as seen in Figure 5b. This property generally decreased in both structures by increasing the radius of double-walled nanotube despite some ups and downs. For the zigzag structures, it can be observed that as the radius increased, the failure stress of the zigzag DWCNTs remained virtually unchanged, while the failure stress of $DWBC_3NT$ with the same chirality dropped sharply to the lowest value obtained among all the double-walled nanotubes studied (135.81GPa). The highest failure stress of $DWBC_3NT$ was obtained 422.77 GPa and 285.74 GPa, obtained for structures (4,4),(8,8) and (8,0),(16,0), respectively, and this property decreased by about 50% and 11% in zigzag and armchair $DWBC_3NT$, respectively.

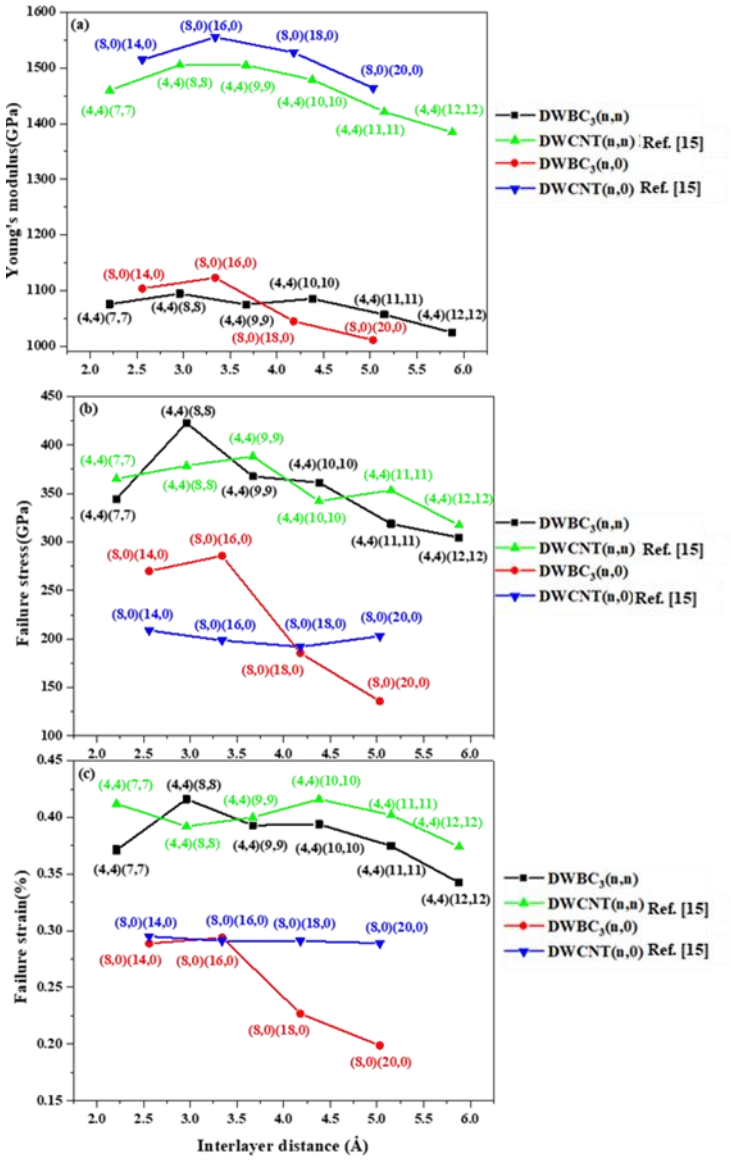

Figure 5. (a) Young's modulus, **(b)** failure stress and **(c)** failure strain of armchair and zigzag DWBC$_3$NTs 300K and their corresponding reference DWCNT from [15].

Besides, the examination of Figure 5c reveals that the failure strain of the armchair DWCNTs and DWBC$_3$NTs did not change significantly with the increase in the radius of the nanotubes. However, like the failure stress, the failure strain of zigzag DWBC$_3$NTs decreased significantly (10%) as the radius of the nanotubes increases. The failure strain of the armchair DWBC$_3$NT was nearly twice as high as that obtained for the corresponding zigzag DWBC$_3$NT, and the highest failure strain of DWBC$_3$NT was 0.416% and 0.293%,

calculated for structures (4,4),(8,8) and (8,0),(16,0), respectively, similar to the failure stress. The results obtained for the armchair and zigzag DWBC3NT and DWCNT are summarized in Tables S4 and S5.

3.3. Effect of adding walls on the Young's modulus of BC_3NTs

In order to measure the mechanical properties of BC_3NTs with respect to the number of walls, a third wall was added to the $DWBC_3NT$ and a zigzag and an armchair $TWBC_3NT$ were modeled, while the results of the corresponding reference TWCNT of similar radius were used (from [15]). In other words, the main objective of this section is to examine how the addition of the second and third walls to a selected zigzag and armchair single-walled BC_3NT could affect its Young's modulus. To this end, (4,4)(8,8)(12,12) armchair and (8,0)(14,0)(20,0) zigzag $TWBC_3NTs$ were modeled and tested under the same loading conditions at a constant temperature of 300K. A schematic view of the designed structures is shown in Figure S5, and the corresponding results are given in Table S6.

According to Figure 6, comparisons were made between the Young's modulus of BC_3NTs having one, two, and three walls. In this figure, the Young's modulus of both zigzag and armchair $SWBC_3NT$ increased significantly as the number of walls increased from one to two and then to three. The addition of one wall to a (4,4) $SWBC_3NT$ improved its Young's modulus by about 33% (from 724.8 GPa to 1094.4 GPa), and the addition of another wall further increased the Young's modulus of the (4,4),(8,8) armchair structure by about 27%, reaching 1505.9 GPa in the structure (4,4),(8,8),(12,12), so that its total increase was about 60%. Similarly, the modulus of the zigzag (8,0) $SWBC_3NT$ first increased by 34% to reach 1103.5 GPa in the (8,0),(14,0) structure, followed by a further improvement of 21% to 1404.4 GPa in the (8,0),(14,0),(20,0) structure. The same behavior was observed for TWCNTs confirms the reasonableness of the results presented. The results obtained demonstrate that increasing the number of walls has a synergistic effect on the Young's

modulus of the considered BC_3NT, so that it could have the same effect on other BC_3NTs of different dimensions by adding more walls.

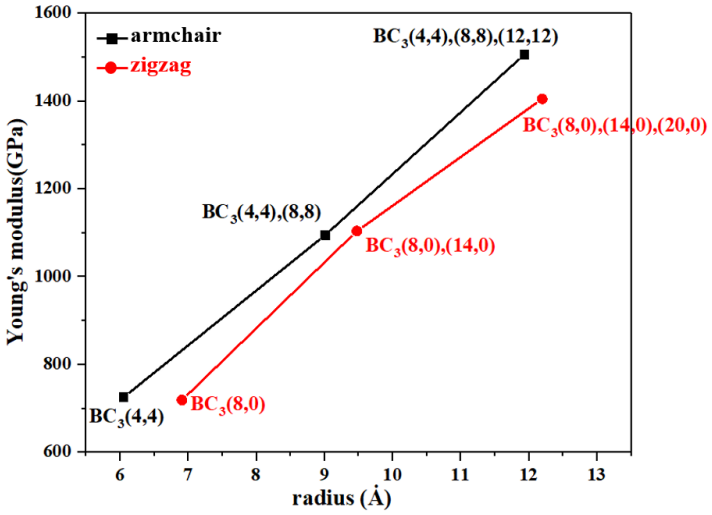

Figure 6. Young's modulus as a function of dimensions for different chiral single-, double- and triple-walled BC_3NT.

3.4. Mechanical properties of BC_3 nanobuds

Recently, 3D nanostructures have received more attention. Nanobuds are a class of 3D nanostructures that form once a fullerene or nanocage is attached to the outer surface of a nanotube or graphene sheet. Research shows remarkable properties and applications of nanobuds due to their porous shells and nanometric thickness [27-29]. In the present study, C_{60} fullerene was selected to model BC_3 nanobuds by attaching one, two, three and four C_{60} to the outer surface of $SWBC_3NT$. An armchair and a zigzag single-walled BC_3NTs with the closest dimension, having (10,10) and (18,0) structures, respectively, were selected to model nanobuds. These structures were selected because they have the closest dimensions when we compared the dimensions of all the armchair and zigzag single-walled structures. Thus, we were able to provide results that could be better compared. All samples were tested under the same loading condition at a constant temperature of 300K. The graphs of the Young's modulus, failure stress, and failure strain obtained in Figure 7 show that all properties consistently decreased as the number of the attached fullerenes increased, whether

in armchair or zigzag chirality. This could be associated with the concentration of stresses that exist around the regions where bonds form between the fullerene and the surface of the nanotube. The higher the number of fullerenes, the higher the stress concentration and the more the mechanical properties are degraded.

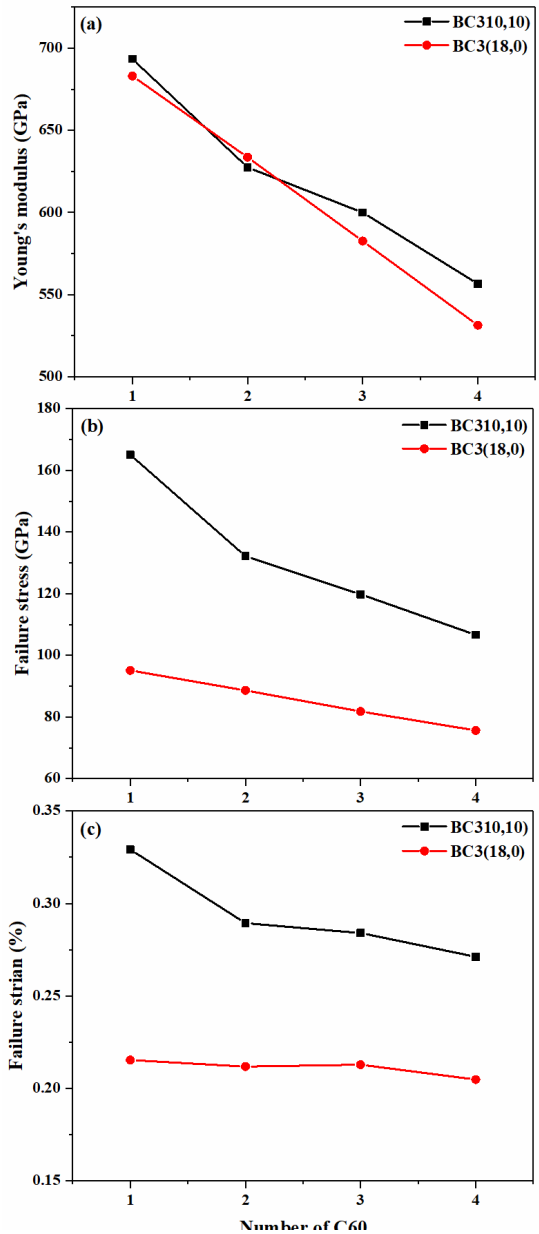

Figure 7. (a) Young's modulus, **(b)** failure stress, and **(c)** failure strain of BC_3 nanobuds under uniaxial tensile tests at 300K.

The Young's modulus, failure stress and failure strain of the armchair BC_3 nanobuds were higher than for zigzag BC_3 nanobuds with the same number of fullerenes attached. In

addition, all mechanical properties of the armchair and zigzag nanobuds were less than or nearly identical to (except for the failure strain of zigzag-1C_{60}) the corresponding SWBC_3NT. The highest Young's modulus of the armchair and zigzag BC_3 nanobuds was 693.4 GPa and 680 GPa, respectively, found in BC_3-1C_{60} structures, and the lowest modulus obtained was observed in BC_3-4C_{60} armchair and zigzag nanobuds with values of 556.6 GPa and 531.4 GPa. Both values were approximately 28% lower than the armchair and zigzag SWBC_3NT. The same percentage reduction was found by comparing the failure stress of zigzag BC_3-4C_{60} nanobuds with that of the corresponding SWBC_3NT (28%), while the failure stress of the armchair BC_3-4C_{60} was remarkably lower (nearly 60%) than that of the corresponding SWBC_3NT (106.62 GPa against 265.52 GPa).

Similar results were reported in previous articles concerning other types of nanobuds. Thus, Ghorbanzadeh et al. [30] used DFT calculations to compare the mechanical properties of simple CNTs and CNT nanobuds. They found a tendency for the Young's modulus of zigzag and armchair CNTs to decrease after attaching one C_{60} molecule. Mashhadzadeh et al. [31] reported in their DFT-based research that the Young's modulus of BeO nanobuds decreased considerably by increasing the number of attached nanocages. All values obtained for the mechanical properties of BC_3 nanobuds are shown in Table S7.

An overview of the failure process of a (18,0)-2C_{60} nanobud under continuous tensile loading is provided in Figure 8. As can be seen, the failure started in the regions close to the attached fullerene molecules, due to higher concentration of stresses in these areas, which facilitates and accelerates crack formation and propagation.

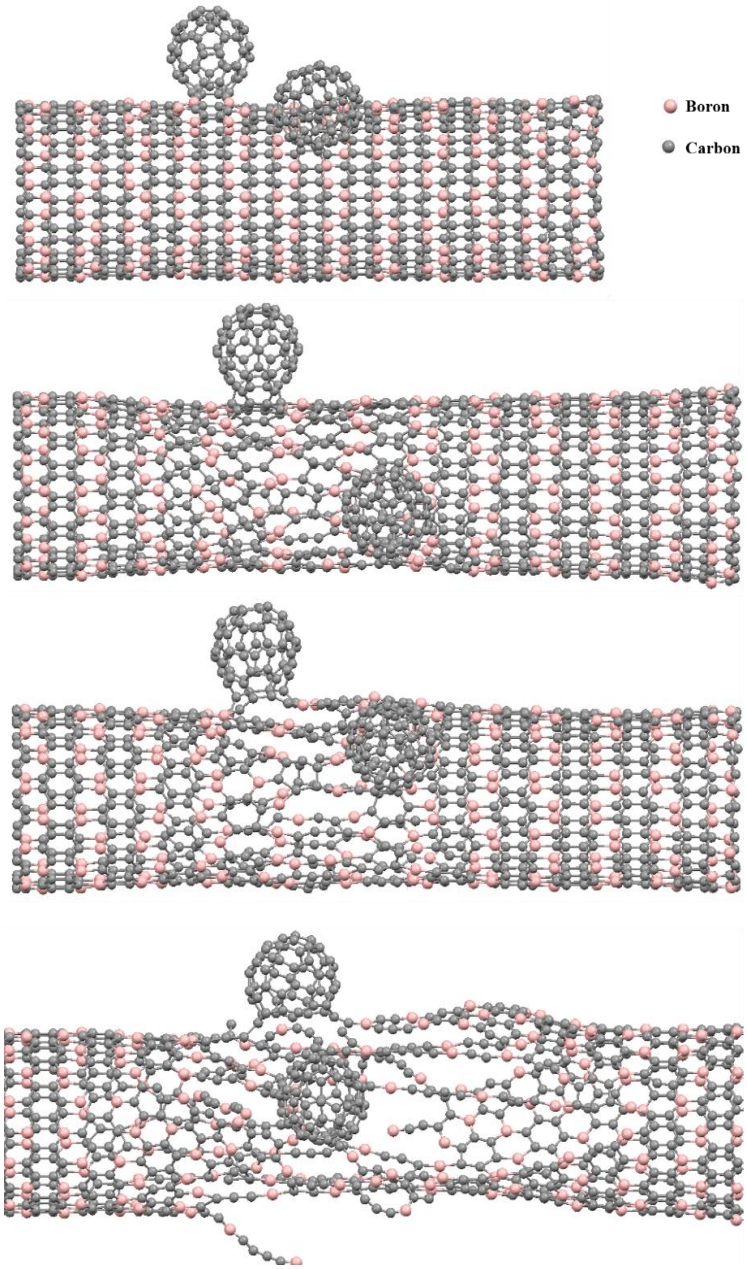

Figure 8. A snapshots of the failure process of a (18,0)-2C_{60} BC_3 nanobud.

302

303 *3.5. Mechanical properties of defective BC_3NT*

304 Finally, we investigated the mechanical properties of (10,10) armchair and (18,0) zigzag
305 SWBC_3NT with point defects, including vacancies and Stone-Wales defects. Just as in the
306 previous subsection, these structures were selected because of their very close dimensions,
307 thus providing easy comparison. Schematic views of the modeled defective structures are
308 shown in Figure 9. This figure shows two types of Stone-Wales defects: type one (STW-1)

forms when a horizontal B-C (or C-C) bond rotates 90 degrees, and type 2 (STW-2) forms when a skewed B-C (or C-C) bond rotates 90 degrees. The results calculated after testing all samples at the constant temperature of 300K are presented in Figure 10 as bar graphs.

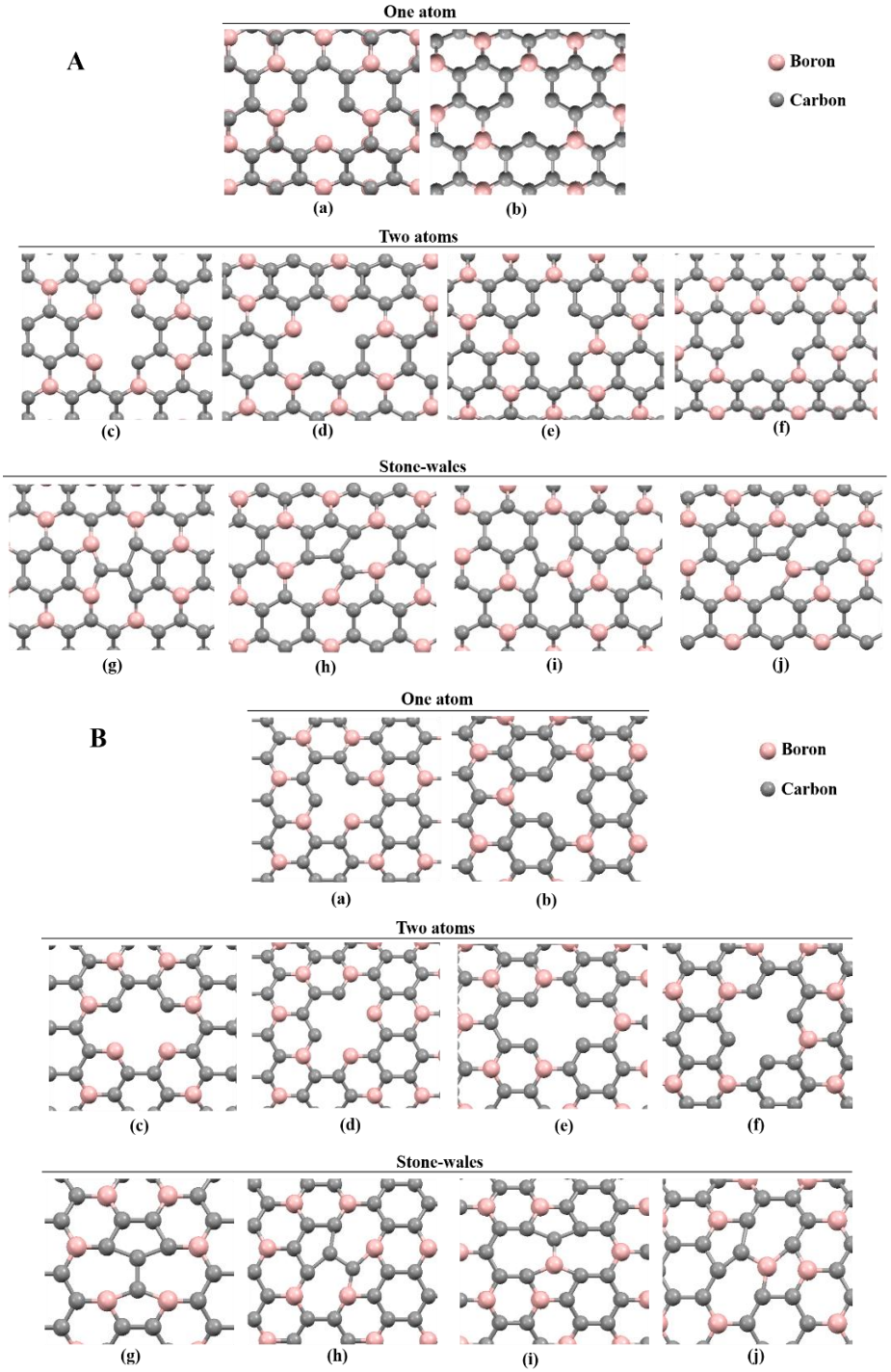

Figure 9. (A) Embedded defects in armchair BC_3NTs: **(a)** one carbon atom vacancy, **(b)** one boron atom vacancy, **(c)** and **(d)** two carbon atoms vacancy, **(e)** and **(f)** one-carbon, one-boron vacancy, **(g)** and **(i)** Stone-wales type 1, (**h**) and (**j**) Stone-wales type 2. **(B)** Same as (A) but for zigzag BC_3NTs.

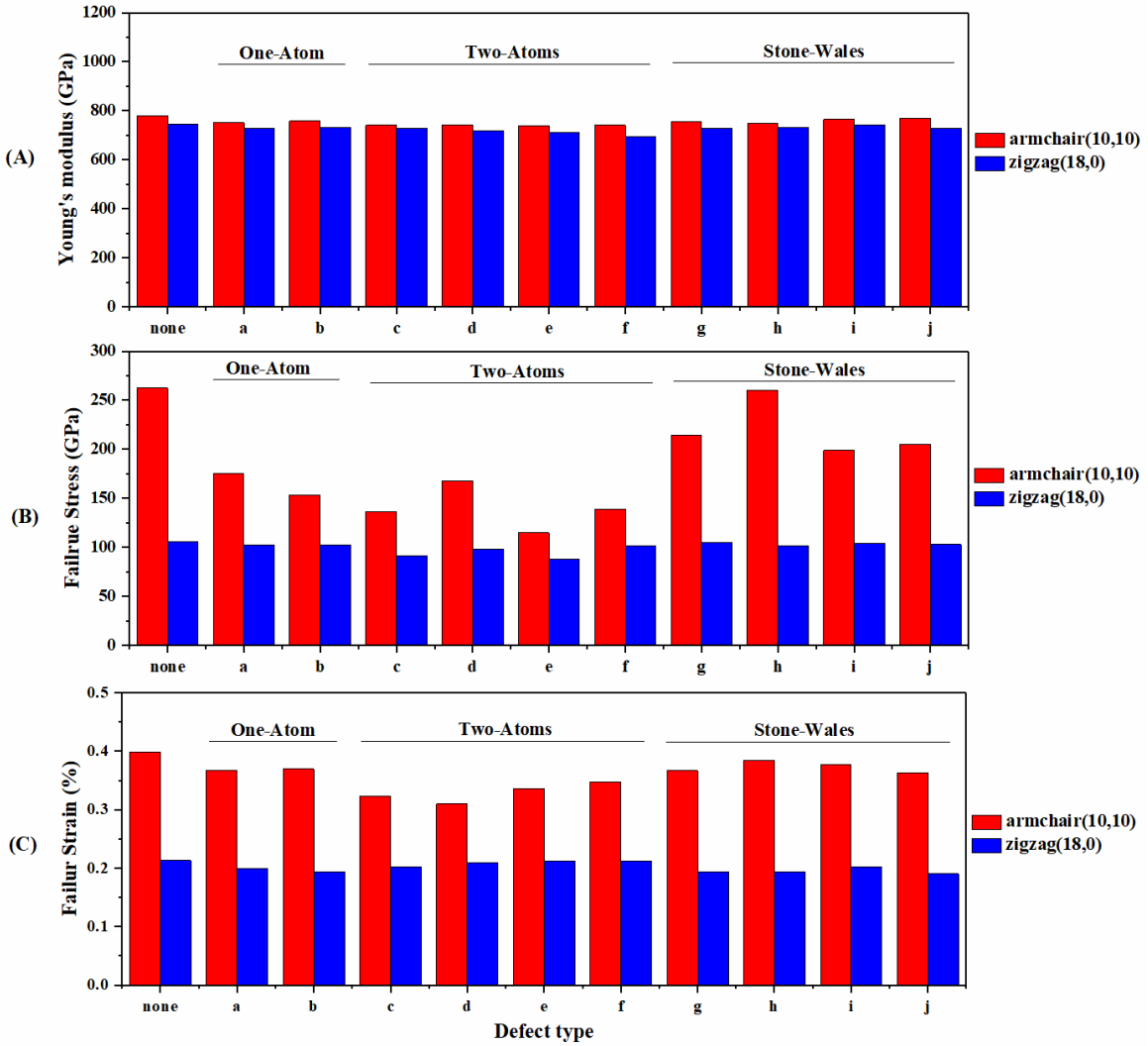

Figure 10. (a) Young's modulus, **(b)** failure stress, and **(c)** failure strain of defective (10,10) BC_3NT and (18,0) BC_3NT.

318

319 It can be seen that the mechanical properties of defective BC_3NTs were lower than for
320 flawless $SWBC_3NTs$, regardless of chirality. The variation in properties regarding the
321 number of missing atoms or the type of the Stone-Wales defect was rather limited and the
322 values obtained for each chirality were very close. BC_3NTs with a Stone-Wales defect had
323 the smallest reduction in Young's modulus and failure stress, whatever the chirality, while
324 the two atom vacancies imposed the maximum reduction in these properties. In addition, the
325 failure strain of the defective armchair BC_3NT with two missing atoms showed a greater
326 reduction than with only one missing atom or with Stone-Wales defects, while in zigzag

structures we found a greater reduction in the failure strain of BC_3NT with Stone-Wales defects compared to those containing atom vacancies. The highest Young's modulus, failure stress, and failure strain calculated for defective BC_3NTs of armchair structure with defect types j (STW-2) and h (STW-1) were 769.1 GPa, 260.32 GPa and 0.384%, respectively. In contrast, the lowest Young's modulus and failure stress of all studied defective BC_3NT were found for zigzag structures with defect type e (one-carbon, one-boron): 711.2 GPa and 87.16 GPa, respectively. Zigzag BC_3NT with defect type j had the lowest failure strain of 0.19%. All the values obtained for the mechanical properties of defective BC_3NT are shown in Table S8.

Previous research has also provided the same kind of results. Thus, Zahedi et al. investigated the effects of crack- and notch-type defects on the mechanical properties of BC_3 single layers and reported a greater reduction in tensile strength properties as crack or notch dimensions increased [24]. In their paper on molecular dynamics, Albooye et al. [18] demonstrated that the Young's modulus of defective BNNT was reduced by increasing the number of missing atoms, with the highest modulus being found in pristine structures while the lowest modulus was reported for structures with three-atom vacancies. In another MD-based research, Gupta et al. [32] studied the Young's modulus, failure stress, and failure strain of hybrid graphene single-layers and showed a downward trend in all the properties mentioned by creating Stone-Wales and nanopore defects compared to pristine single-layer graphene. Ghorbanzadeh et al. [33] investigated the effects of point defects on the properties of ZnO graphene-like surfaces in a DFT study, and also reported the negative effect of point defects on the mechanical properties of this material. Figure 11 presents a snapshot of the failure process of a (10,10) armchair BC_3NT with two atom vacancies (defect type e). As expected, the failure occurred in the defective areas due to the higher stress concentration, and the process continued until the destruction of the nanostructure was complete.

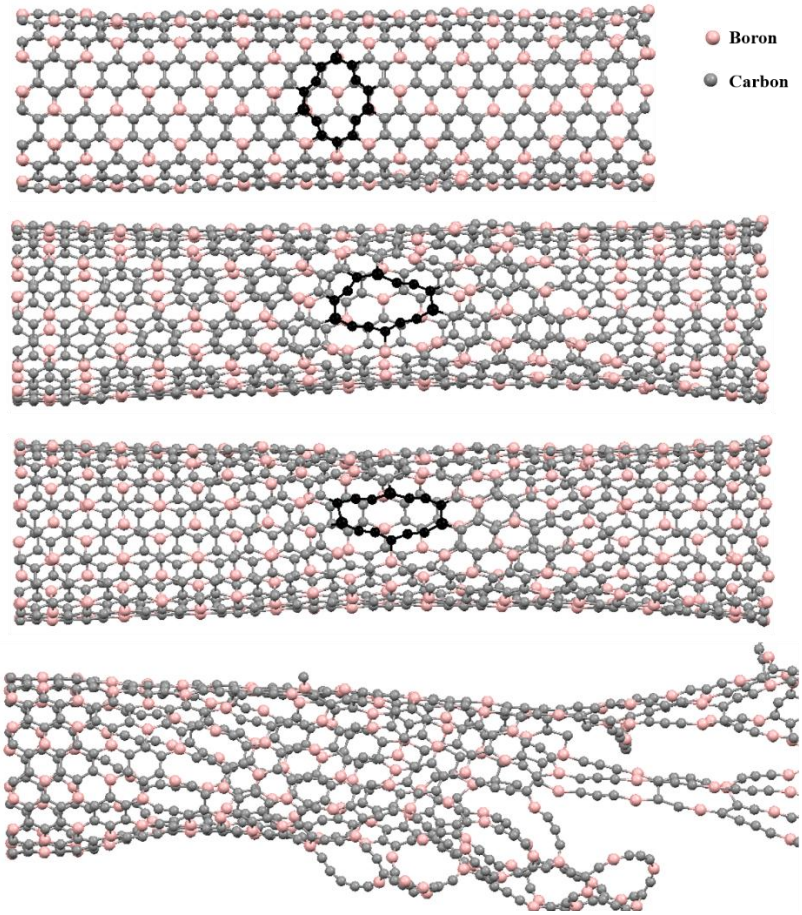

Figure 11. Snapshot of the failure process of an armchair (10,10) BC_3NT with two-atom defects (defect type e).

352

353 **4. Conclusions**

354 In the present article, molecular dynamics (MD) simulation was used to study the
355 mechanical properties of BC_3 nanotubes. We examined the Young's modulus, failure stress
356 and failure strain of BC_3NT, BC_3 nanobuds and BC_3NT with different types of defects as a
357 function of factors such as chirality, size, number of walls and temperature. We also used the
358 results of CNTs of similar chirality and dimensions, obtained from a previous work, to
359 compare and validate the present results. Our results demonstrated that the addition of walls
360 to single-walled BC_3NT increased the Young's modulus, failure stress, and failure strain
361 remarkably, regardless of chirality, so that triple-walled BC_3NT had markedly better

properties than double-walled nanotubes, and double-walled nanotubes showed better properties compared to single-walled ones, again regardless of chirality. The highest Young's modulus obtained was observed for $TWBC_3NT$ and the lowest modulus was calculated for $SWBC_3NTs$. In addition, armchair structures had higher mechanical properties than zigzag structures in most of the nanotubes studied, and BC_3NT had lower properties compared to CNTs. The highest Young's modulus of the armchair and zigzag $SWBC_3NT$ was calculated to be 780.5 GPa and 751.7 GPa for (10,10) and (16,0) structures, respectively. The modeling of double and triple-walled BC_3NTs based on structures (4,4) and (8,0), with the closest radius, revealed that the Young's modulus of the armchair (4,4),(8,8),(12,12) $TWBC_3NT$ and (4,4),(8,8) $DWBC_3NT$ was nearly 60% and 33% higher than (4,4) $SWBC_3NTs$, respectively. Similarly, the Young's modulus of the zigzag (8,0),(14,0),(20,0) $TWBC_3NT$ and (8,0),(14,0) $DWBC_3NT$ was 55% and 34% higher than that of (8,0) $SWBC_3NT$, respectively.

Furthermore, after modeling BC_3 nanobuds by attaching 1 to 4 C_{60} molecules to the outer surface of $SWBC_3NT$, we observed that all mechanical properties were slightly reduced by increasing the number of attached fullerenes. Thus, the lowest Young's modulus, failure stress and failure strain of each chirality were obtained in nanobuds with four attached fullerenes. The lowest Young's modulus of the armchair and zigzag BC_3 nanobuds was calculated at 556.6 GPa and 531.4 GPa for structures (10,10)-$4C_{60}$ and (18,0)-$4C_{60}$, respectively, and were 28% and 30% lower than the corresponding pristine $SWBC_3NTs$, respectively. In the end, we modeled and tested $SWBC_3NTs$ with embedded one-atom and two-atom vacancies as well as Stone-Wales defects and found that Stone-Wales defects imposed the smallest reduction in Young's modulus and failure stress, regardless of chirality, while two-atom vacancies resulted in the largest reduction in these properties. With respect to failure strain, the greatest reduction was observed for two-atom vacancies and Stone-Wales

defects in the case of armchair and zigzag structures, respectively. We calculated the highest Young's modulus, failure stress, and failure strain of the defective BC_3NTs in armchair structures with defect types j (STW-2) and h (STW-1), and the corresponding values were 769.1 GPa, 260.32 GPa, and 0.384%, respectively. Overall, the outstanding results of this study could provide a new prospect for the wider use of 1D carbon-based materials in a variety of applications.

Data availability

The raw/processed data required to reproduce these findings cannot be shared at this time as the data also forms part of an ongoing study.

References

1. Saeed, K. and I. Khan, *Carbon nanotubes-properties and applications: a review.* Carbon letters, 2013. **14**.
2. Rao, R., et al., *Carbon Nanotubes and Related Nanomaterials: Critical Advances and Challenges for Synthesis toward Mainstream Commercial Applications.* ACS Nano, 2018. **12**(12): p. 11756-11784.
3. Talla, J.A. and A.A. Ghozlan, *Effect of boron and nitrogen co-doping on CNT's electrical properties: Density functional theory.* Chinese Journal of Physics, 2018. **56**(2): p. 740-746.
4. Chen, S.C., et al., *Optical properties of BC3 nanotubes.* Journal of Vacuum Science & Technology B: Microelectronics and Nanometer Structures Processing, Measurement, and Phenomena, 2006. **24**(1): p. 46-49.
5. Miyamoto, Y., et al., *Electronic properties of tubule forms of hexagonal ${\mathrm{BC}}_{3}$.* Physical Review B, 1994. **50**(24): p. 18360-18366.
6. Jana, D., et al., *Effect of chemical doping of boron and nitrogen on the electronic, optical, and electrochemical properties of carbon nanotubes.* Progress in Materials Science, 2013. **58**(5): p. 565-635.
7. Wei, B., et al., *Electrical transport in pure and boron-doped carbon nanotubes.* Applied Physics Letters, 1999. **74**(21): p. 3149-3151.
8. Zhang, H., et al., *Theoretical Studies on the Electronic and Optical Properties of Honeycomb BC(3) monolayer: A Promising Candidate for Metal-free Photocatalysts.* ACS omega, 2018. **3**(9): p. 10517-10525.
9. Zhao, J. and R.-H. Xie, *Electronic and Photonic Properties of Doped Carbon Nanotubes.* Journal of nanoscience and nanotechnology, 2004. **3**: p. 459-78.
10. Borowiak-Palen, E., et al., *Formation of novel nanostructures using carbon nanotubes as a frame.* Synthetic Metals, 2005. **153**(1): p. 345-348.
11. Tomanek, D., et al., *Calculation of electronic and structural properties of BC3.* Phys Rev B Condens Matter, 1988. **37**(6): p. 3134-3136.
12. Tanaka, H., et al., *Novel macroscopic BC3 honeycomb sheet.* Solid State Communications, 2005. **136**(1): p. 22-25.

13. Dadrasi, A., A.R. Albooyeh, and A. Hamed Mashhadzadeh, *Mechanical properties of silicon-germanium nanotubes: A molecular dynamics study.* Applied Surface Science, 2019. **498**: p. 143867.
14. Memarian, F., et al., *Molecular dynamic study of mechanical properties of single/double wall SiCNTs: Consideration temperature, diameter and interlayer distance.* Vacuum, 2017. **139**: p. 93-100.
15. Salmankhani, A., et al., *Mechanical Properties of C3N Nanotubes from Molecular Dynamics Simulation Studies.* Nanomaterials, 2020. **10**(5).
16. Lindsay, L. and D. Broido, *Optimized Tersoff and Brenner empirical potential parameters for lattice dynamics and phonon thermal transport in carbon nanotubes and graphene.* Physical Review B, 2010. **81**(20): p. 205441.
17. Kınacı, A., et al., *Thermal conductivity of BN-C nanostructures.* Physical Review B, 2012. **86**(11): p. 115410.
18. Albooyeh, A.R., A. Dadrasi, and A.H. Mashhadzadeh, *Effect of point defects and low-density carbon-doped on mechanical properties of BNNTs: A molecular dynamics study.* Materials Chemistry and Physics, 2020. **239**: p. 122107.
19. Van Lier, G., et al., *Ab initio study of the elastic properties of single-walled carbon nanotubes and graphene.* Chemical Physics Letters, 2000. **326**(1): p. 181-185.
20. Hsieh, J.-Y., et al., *Theoretical variations in the Young's modulus of single-walled carbon nanotubes with tube radius and temperature: A molecular dynamics study.* Nanotechnology, 2006. **17**: p. 3920.
21. Mohammadpour, E., M.Z. Abdullah, and M. Awang, *Predicting the Young's Modulus of Single-Walled Carbon Nanotubes using Finite Element Modeling.* Journal of Applied Sciences, 2011. **11**: p. 1653-1657.
22. Yu, M.-F., et al., *Tensile Loading of Ropes of Single Wall Carbon Nanotubes and their Mechanical Properties.* Physical Review Letters, 2000. **84**(24): p. 5552-5555.
23. Treacy, M.M.J., T.W. Ebbesen, and J.M. Gibson, *Exceptionally high Young's modulus observed for individual carbon nanotubes.* Nature, 1996. **381**(6584): p. 678-680.
24. Khademi-Zahedi, R., *Mechanical properties of graphene-like BC3; a molecular dynamics study.* Computational Materials Science, 2019. **168**: p. 1-10.
25. Badehian, H.A. and K. Gharbavi, *Transport and mechanical properties of double-walled carbon nanotubes as a function of interwall distance.* Molecular Crystals and Liquid Crystals, 2017. **650**(1): p. 138-146.
26. Doh, J. and J. Lee, *Prediction of the mechanical behavior of double walled-CNTs using a molecular mechanics-based finite element method: Effects of chirality.* Computers & Structures, 2016. **169**: p. 91-100.
27. Qi, J., et al., *Multi-shelled hollow micro-/nanostructures.* Chemical Society Reviews, 2015. **44**(19): p. 6749-6773.
28. Ashrafian, S., et al., *Greatly enhanced adsorption of platinum on periodic graphene nanobuds: A first-principles study.* Applied Surface Science, 2015. **351**: p. 1105-1115.
29. Ghahghaei Nezam Abadee, Z., M. Hekmati, and M.D. Ganji, *Removing phenol contaminants from wastewater using graphene nanobuds: DFT and reactive MD simulation investigations.* Journal of Molecular Liquids, 2019. **286**: p. 110872.
30. Ghorbanzadeh Ahangari, M., M.D. Ganji, and F. Montazar, *Mechanical and electronic properties of carbon nanobuds: First-principles study.* Solid State Communications, 2015. **203**: p. 58-62.
31. Hamed Mashhadzadeh, A., et al., *Theoretical studies on the mechanical and electronic properties of 2D and 3D structures of Beryllium-Oxide graphene and graphene nanobud.* Applied Surface Science, 2019. **476**: p. 36-48.
32. Kumar Gupta, K., et al., *Probing the compound effect of spatially varying intrinsic defects and doping on mechanical properties of hybrid graphene monolayers.* Journal of Materials Science & Technology, 2020.

33. Ahangari, M.G., et al., *Effect of various defects on mechanical and electronic properties of zinc-oxide graphene-like structure: A DFT study*. Vacuum, 2019. **165**: p. 26-34.